LANGMUIR

Article

pubs.acs.org/Langmuir

CO_2-Reactive Ionic Liquid Surfactants for the Control of Colloidal Morphology

Paul Brown,[†,#] Vishnu Sresht,[†,#] Burak H. Eral,[†] Andrew Fiore,[†] César de la Fuente-Núñez,[‡,§,∥] Marcus O'Mahony,[†] Gabriel P. Mendes,[†] William T. Heller,[⊥] Patrick S. Doyle,[†] Daniel Blankschtein,[†] and T. Alan Hatton*[,†]

[†]Department of Chemical Engineering and [‡]Synthetic Biology Group, MIT Synthetic Biology Center, Research Laboratory of Electronics, Department of Biological Engineering, Department of Electrical Engineering and Computer Science, Massachusetts Institute of Technology, Cambridge, Massachusetts 02139, United States

[§]Eli and Edythe L. Broad Institute of MIT and Harvard, 415 Main Street, Cambridge, Massachusetts 02142, United States

[∥]Harvard Biophysics Program, Harvard University, Cambridge, Massachusetts 02138, United States

[⊥]Biology and Soft Matter Division, Neutron Sciences Directorate, Oak Ridge National Laboratory, Oak Ridge, Tennessee 37831, United States

Supporting Information

ABSTRACT: This article reports on a new class of stimuli-responsive surfactant generated from commercially available amphiphiles such as dodecyltrimethylammmonium bromide (DTAB) by substitution of the halide counterion with counterions such as 2-cyanopyrrolide, 1,2,3-triazolide, and *L*-proline that complex reversibly with CO_2. Through a combination of small-angle neutron scattering (SANS), electrical conductivity measurements, thermal gravimetric analysis, and molecular dynamics simulations, we show how small changes in charge reorganization and counterion shape and size induced by complexation with CO_2 allow for fine-tunability of surfactant properties. We then use these findings to demonstrate a range of potential practical uses, from manipulating microemulsion droplet morphology to controlling micellar and vesicular aggregation. In particular, we focus on the binding of these surfactants to DNA and the reversible compaction of surfactant−DNA complexes upon alternate bubbling of the solution with CO_2 and N_2.

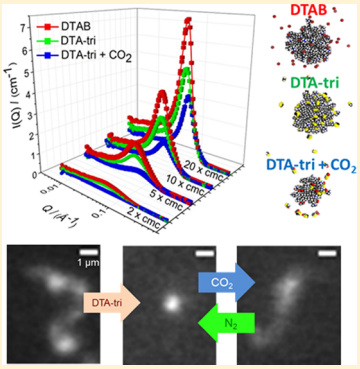

INTRODUCTION

Surfactants play a pivotal role in the physical, biological, and chemical sciences, with a world market of US $33 billion.[1] Their amphiphilicity makes them the molecules of choice in materials and biological science to generate self-assembled structures, stabilize interfaces, affect the solubilization and morphology of nanomaterials, and manipulate biological and physicochemical properties such as interfacial tension and viscosity.

Stimuli-responsive surfactants improve upon their non-responsive counterparts by acting as levers between important microscale and macroscale system properties and readily controllable external stimuli.[2] Conventionally, control of surfactant properties is achieved through variations in surfactant concentration, ionic strength, and pH, leading to irreversible changes in system composition and phase stability. A change in temperature may also be used to manipulate the surfactant properties. However, on a large scale, this requires significant energy input, and for certain biological applications, it may adversely affect the activity and conformation of biomolecules. A more sophisticated approach involves the use of external stimuli to actuate changes in the surfactant architecture, manifested as changes in the overall system properties, which promises to allow for the recycling of surfactant and lower costs. However, the manufacturing of stimuli-responsive surfactants is still prohibitively expensive, thereby precluding a wider range of potential applications. With the above need in mind, we introduce novel CO_2-reactive ionic liquid surfactants that are synthesized from a plentiful supply of commercially available and inexpensive starting materials (Figure 1) and whose properties may be controlled reversibly simply by bubbling CO_2 or N_2 through their solution.

The first reported CO_2-switchable surfactant was based on the reaction of CO_2 with a built-in amidine functional group.[3] Here, the nonionic (non-surface-active) *N*′-hexadecyl-*N*,*N*-dimethylacetamidine compounds were converted to charged *N*′-hexyldecyl-*N*,*N*-dimethylacetamidinium bicarbonate surfactants after bubbling the solution with CO_2. This process altered the pH of the solution and produced a surfactant. Other approaches, including the use of amines to form zwitterionic adducts or ammonium carbamates, have recently received considerable attention because the stimulating agent, CO_2,

Received: March 1, 2017
Revised: July 11, 2017
Published: July 12, 2017

DOI: 10.1021/acs.langmuir.7b00679
Langmuir 2017, 33, 7633−7641

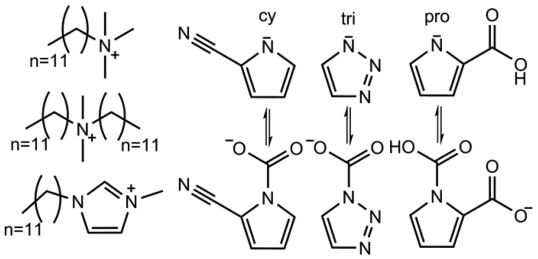

Figure 1. Compounds investigated and the reaction of each anion with CO_2. Cations are (from top to bottom) dodecyltrimethylammonium, didodecyldimethylammonium, and 1-dodecyl-3-methylimidazolium. Anions are (from left to right) 2-cyanopyrrolide (cy), 1,2,3-triazolide (tri), and L-proline (pro).

exhibits good biocompatibility and is nontoxic and abundant.[4] At the molecular level, however, the mechanisms generally rely on controlling the head or the tail of the surfactant rather than the counterion, thereby limiting the range of applications in which they can be exploited. Responsive counterions have been reported before,[2] but never those that react to CO_2. In this work, through a combination of molecular dynamics (MD) simulations and various experimental methods, we investigate surfactants generated from reactive ionic liquids in which the fine-tuning of electrostatics, packing parameters, and the surrounding hydrogen bond network are all possible, resulting in substantial responses on the macroscale. To demonstrate potential practical uses, we show that the new CO_2-responsive surfactants can be utilized in a number of colloidal systems. In particular, we demonstrate surfactant binding to DNA and reversible compaction upon bubbling alternately with CO_2 and N_2.

It is well established that the helical structure of DNA and its effective compaction can be achieved by the addition of complexing cationic agents such as DTAB, whereby isolated DNA chains undergo a discrete coil−globule transition in solution, even at very low surfactant concentrations (well below the surfactant critical micelle concentration (cmc)).[5] The subsequent decompaction has previously relied on cyclodextrin additives,[6] which irreversibly affect the composition of the system, or on the use of photoresponsive surfactants.[7] Photoresponsive surfactants require complex synthesis and the use of actinic light, which may be harmful to biological materials and which also decays rapidly over long distances or in media with a large refractive index such as emulsions, hydrogels, and tissue. In contrast, the use of CO_2-reactive surfactants to increase the transfection efficiency is particularly attractive in areas of biotechnology and in DNA-based chemistry, with further potential for the reversible control of protein (or other biomolecule) folding.

EXPERIMENTAL SECTION

Materials and Methods. Dodecyltrimethylammonium bromide (99%, DTAB), didodecyldimethylammonium bromide (99%, DDAB), 1-methylimidazole (99%), 1-bromododecane (>97%), pyrrole-2-carbonitrile (96%, cy), 1*H*-1,2,3-triazole (97%, tri), L-proline (>99%, pro), trizma base (99.9% titration), and ethylenediaminetetraacetic acid (99%, EDTA) were purchased from Sigma-Aldrich and used without further purification. Cyclohexane (99.9) was purified (Supporting Information). 1-Methyl-3-dodecylimidazolium bromide (C_{12}mimBr) was synthesized by mixing equimolar amounts of 1-methylimidazole and 1-bromododecane in acetonitrile followed by refluxing overnight. The resulting white solid was washed with ether. CO_2-reactive surfactants were synthesized by converting the halide ion through an ion-exchange technique using a strong ion-exchange resin (Dowex 550A) as follows: 1 equiv of surfactant (typically ∼80 mmol) was dissolved in EtOH/H_2O (1:1 v/v) and passed through a column (30 cm × 1 cm^2) of the prewashed resin. The hydroxide form of the surfactant then reacted with an aqueous solution (1 equiv) of the appropriate counterion. The solvent was removed by evaporation and drying in vacuo for 48 h. The synthesized compounds were characterized by ^{1}H NMR, with the observed shifts consistent with expected values (Supporting Information), and the loss of bromide ions was observed using elemental analysis.

Electrical Conductivity (κs). The electrical conductivities were determined using a Jenway model 4510 conductivity/TDA conductivity meter, with the temperature controlled at 25 ± 0.1 °C (thermostatic water bath). Critical micelle concentrations were calculated from break points between the high {dκ/d(conc)} and the low {dκ/d(conc)} branches of behavior.

SANS Measurements. Small-angle neutron scattering was carried out at BL-6B (EQSANS), Spallation Neutron Source, ORNL, Oak Ridge, TN.[8] Measurements were carried out using sample-to-detector distances of 1.3 and 4 m, which collectively probe a range of momentum transfers from 0.004 to 0.6 $Å^{-1}$. Data reduction followed standard procedures, and the reduced data were normalized to give the absolute scattering cross section, I(Q) (cm^{-1}), as a function of momentum transfer, Q ($Å^{-1}$). Surfactant samples were prepared at 2/5/10/20 × cmc using deuterium oxide (D_2O), (scattering length density ρ = 6.38 × 10^{10} cm^{-2}) to provide the necessary contrast and were placed in Starna fused silica cuvettes (path length 2 mm). A low level of residual incoherent scattering was accounted for by a small flat background term in the data analysis. Data were analyzed in absolute units ($I(Q)/cm^{-1}$) with fitted scale factors consistent with expectations based on sample compositions. Data were analyzed by model fitting (Supporting Information), whereas microemulsion and polymer structural parameters were extracted using Porod analysis and model fitting (Supporting Information). Microemulsion pseudo-phase-diagram preparation is also detailed in the Supporting Information.

Surface Tension. The surface tension between aqueous surfactant solutions (2 × cmc) and air was measured at 25 ± 1 °C using a Krüss drop shape analysis DSA1 apparatus. This instrument obtains spatial coordinates of a drop edge (shape and size), which are then used to calculate the surface tension. Measurements were acquired until steady values of the surface tension were reached. The calibration used the surface tension of pure water (Millipore, 18 MΩ).

Melting Points. Each melting point was measured using a TA Instruments DSC Q2000. The heating ramp for each sample was 10 °C min^{-1}.

Dynamic Light Scattering. Dynamic light scattering measurements were carried out to define the boundaries at which DNA compaction occurred. DLS measurements were carried out on a Brookhaven Instruments NanoBrook ZetaPALS (NY) using a constant scattering angle of 90° at 25 °C. All solutions were made dust-free by filtration through cellulose acetate membranes of 0.45 mm pore size (Millipore, USA). DNA (from salmon sperm, 15632-011, 2000 bp) was purchased from Life Science Technologies (MA).

Circular Dichroism (CD). Circular dichroism spectra were collected on an Aviv Biomedical model 202 CD spectrometer (NJ) in 1.0 cm quartz cuvette cells over a wavelength range of 320 to 220 nm with an integration time of 2 s and 1 nm data intervals.

DNA Visualization. These experiments utilized 165.6 kilo-base pair T4 DNA (Nippon Gene). DNA was diluted from stock concentration using a solution of 4% by volume β-mercaptoethanol (BME, Cabiochem) in 0.5× Tris-borate-EDTA buffer (Sigma-Aldrich) and stained with YOYO-1 intercalating dye (Invitrogen) at a dye ratio of 1 dye molecule per 4 base pairs. Images were taken for a DNA concentration of 0.63 pM (0.0687 μg mL^{-1}) and surfactant concentrations of ∼3.3 mM.

Modeling of the Surfactants. Surfactant modeling was undertaken using force-field forms and parameters that are consistent with the OPLS-AA paradigm. This was done because simulations of surfactant molecules in the bulk and interfacial aqueous environments that utilize the OPLS-AA force field are in good agreement with

DOI: 10.1021/acs.langmuir.7b00679
Langmuir 2017, 33, 7633−7641

experiments.[9,10] Despite their lack of explicit polarizability, OPLS-AA-compatible parameters have been utilized by several authors to study the interactions of halides in, and with, water.[11,12] These simulations are in semiquantitative agreement with, and reproduced interhalide trends are obtained by, studies that have utilized polarizable models. The SPC/E model for water was used in these simulations because of its relatively simple structure and satisfactory reproduction of the aqueous environment around amphiphiles.[13]

Partial charges and dihedral profiles (specifically the O−C−N−C and O−C−N−N dihedrals associated with the complexed CO_2 moiety) in the molecular models of the CO_2-responsive counterions studied here were parametrized per the methodology of Padua and co-workers,[14] whenever these parameters could not be directly obtained from the literature. The N−N−N angle and angular force constant were taken from the study of triazolium-based ionic liquids by Yan et al.[15] Parameters for 2-cyanopyrrolide were obtained from a simulation study by Wu et al.[16] Bond lengths, angles, force constants, and dihedrals pertaining to the CO_2 functional group and its attachment to the counterions were taken from the study on the effect of CO_2 complexation on ionic liquids by Gutowski and Maginn.[17] It must be emphasized that the purpose of the current study is to compute the changes in interfacial and bulk behaviors of the counterions before and after complexation with CO_2. Consequently, we are more interested in comparing the same counterion, with and without the cojoined COO moiety, than we are in comparing behaviors across counterions.

Simulation Methodology. Partial atomic charges for the uncomplexed and complexed counterions were calculated using the CHelpG approach in Gaussian 03[18] with electron densities computed at the MP2/cc-pVTZ(-f) level after an initial geometry optimization carried out at the HF/6-31G(d) level. Partial charge color maps were generated using Avogadro.[19]

The distributions of hydrogen atoms around the counterions and the numbers of hydrogen bonds associated with each counterion in a bulk aqueous environment were calculated by placing a single Na^+-counterion pair in a 4.2 nm × 4.2 nm × 4.2 nm cubic simulation box initialized with 2100 SPC/E water molecules and simulated in the *NpT* ensemble for 2.0 ns.

The potentials of mean force of the counterions as a function of the distance from the vacuum/water interface were calculated using a series of umbrella sampling simulations centered around 21 equispaced points spanning 3.7 nm below and 1.2 nm above the Gibbs dividing surface.[20] These simulations were carried out in 4 nm × 4 nm × 11 nm simulation boxes initialized with 1 Na^+-counterion pair and 1349 SPC/E molecules in an *NVT* ensemble. The depth of the counterion below the interface was collected at intervals of 10 ps over a trajectory of 4 ns, and the resulting position histograms were stitched together using the WHAM algorithm. The surface pressures induced by the counterions were computed from the potentials of mean force using the extended Poisson−Boltzmann approach in combination with the Gibbs adsorption equation following the procedure utilized by Horinek et al.[21]

Each micelle simulation was initialized by inserting a single preformed surfactant micelle of a chosen aggregation number, generated using the approach utilized by Iyer et al.,[22] as well as an appropriate number of counterions, into a 9.5 nm × 9.5 nm × 9.5 nm cubic simulation box containing approximately 24 500 SPC/E molecules. This system was then equilibrated in an *NpT* ensemble for a total of 12 ns. Statistics on the counterion distribution around the micelle were collected from the last 10 ns of each simulation.

All molecular dynamics simulations were carried out with the GROMACS 5.0.2 package.[23] Short-range Coulombic and van der Waals interactions were cut off at 1.2 nm, with the long-ranged Coulombic interactions described using a particle mesh Ewald (PME) summation. Hydrogen bonds were constrained using the LINCS algorithm permitting a time step of 2 ps to be used with a Verlet integrator for all of the simulations. A temperature of 298 K was maintained in all of these simulations using the velocity-rescaled thermostat with a coupling constant of 0.5 ps. Constant-pressure simulations (p = 1.0 bar) were carried out using the Berendson barostat with a coupling constant of 1.0 ps.

RESULTS AND DISCUSSION

Surfactant Physicochemical Properties. The surfactants studied here were synthesized using commercially available and inexpensive starting materials (Figure 1). The driving force for self-aggregation is the hydrophobic effect dominated by the cation, which may be selected from virtually any cationic moiety available. The range of potential anions is equally broad—we investigated a chiral amino acid, L-proline (pro)—to accommodate toxicological considerations and because it has favorable viscosity modification properties and other aprotic heterocyclic anions (triazolide (tri) and 2-cyanopyrrolide (cy)) due to their fast binding kinetics[24] and their reaction with CO_2 according to a 1:1 molar stoichiometry.[25−27] The binding of the ionic liquid surfactants with CO_2 was investigated using thermogravimetric analysis (TGA). The adsorption profiles can be seen in Figure 2. The molar uptake at 25 °C is around

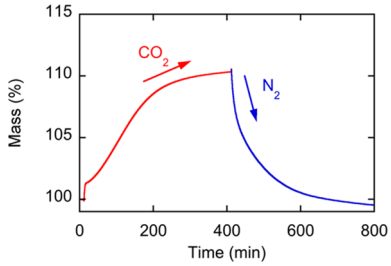

Figure 2. CO_2 absorption/desorption profile for DTA-tri as measured by thermogravimetric analysis at 25 °C and a flow rate of 60 mL min^{-1}.

100 mg of CO_2 per g of IL. This value is around one-third lower than the 1:1 molar absorption anticipated on the basis of stoichiometric considerations, a consequence of the finite, temperature-dependent reversibility of the reaction.[26] The chemical binding and physical binding were easily reversed through a change in the gas to N_2 or upon increases in the temperature. Kinetics were not investigated, but it was evident that the CO_2 absorption in solution was much faster than in the pure ionic liquid.[3]

Charge reorganization over large counterions can have dramatic effects on the affinity of the counterion for other ions[31] and water.[32] In particular, Gutowski and Maginn found that changes in partial charges caused by CO_2 complexation led to a stronger, more extensive, and more persistent hydrogen-bonding network.[17] To investigate whether this effect leads to a change in surfactant physicochemical properties, two of the most fundamental characteristics of ionic surfactants, the critical micelle concentration (cmc) and degree of counterion binding (βs), were determined via electrical conductivity measurements [Figure 3 (see also Figures S1 and S2) and Table 1]. The cmc's can be reduced by exchanging the halides of the inert surfactants (which do not bind to CO_2) with large organic anions. This is surprising because the large organic anions should be less effective at screening cation−cation headgroup repulsions and therefore would be expected to increase the cmc. In general, β increases slightly, which suggests that the larger reactive anions are attracted more strongly to the micelle surface than are the smaller halides. Upon reacting with CO_2, the cmc's change significantly, and, more importantly, large decreases in β are observed, consistent with the ionization of the surfactant. In the case of DTA-tri, the cmc decreases by more than 20%, and β decreases by around two-thirds upon

DOI: 10.1021/acs.langmuir.7b00679
Langmuir 2017, 33, 7633−7641

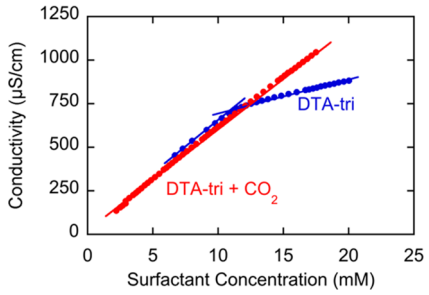

Figure 3. Conductivity data of DTA-tri and DTA-tri + CO_2.

complexation with CO_2. Furthermore, after bubbling with N_2, the desorption of CO_2 occurred with an associated reversal of surfactant properties. It is important to note that for DTAB the cmc does not change upon bubbling with CO_2, although the pH drops from 7.2 to pH 5.4.

The aggregation behavior of these surfactants may be considered in terms of a combination of increasing neutralization of surface charge due to counterion binding, which promotes the formation of micelles at lower surfactant concentrations, and a decreasing entropic penalty when counterions that interact weakly with water condense on the surface of the micelle.

MD simulations reveal significant differences in the interactions of the counterions with water (Figure 4). The radial distribution function of water molecules around an ion provides a convenient means to measure its hydrated radius.[33] The radial distribution function $g(r)$, shown in Figure 4 for counterions tri, cy, and pro, is a measure of the probability of finding a water molecule at a certain distance, r, from the center of mass of the counterion. In the three subplots representing $g(r)$ at the top of Figure 4, the green line, corresponding to uncomplexed counterions, (1) increases from zero at a smaller distance from the center of mass of the counterion and (2) is lower for small values of r than the blue line that corresponds to the CO_2-complexed counterion. Together, these observations indicate that the probabilities of finding water molecules at small values of r around the center of mass of counterions tri, cy, and pro are lower after complexation with CO_2. The addition of the relatively bulky COO moiety to the anion upon complexation with CO_2 significantly increases the hydrated size of all of the counterions.

In contrast to the consistent change in the hydrated radius of the counterions, there is no general trend in the distribution of hydrogen atoms around the counterions; no significant changes are observed in the position and average number of these hydrogen atoms in the first solvation shell around tri and tri + CO_2. Furthermore, there is only a slight difference in the average number of hydrogen bonds associated with these two counterions. This suggests that any disruption of hydrogen-bond networks caused by the occlusion of the nitrogen atom at the complexation site on tri is approximately compensated for by increased hydrogen bonding with the COO moiety. These conclusions are consistent with the slight differences in viscosity observed for triazolide-based ionic liquid solutions containing water before and after CO_2 complexation.[34]

On the other hand, the first solvation shell of hydrogen atoms moves closer to the cy counterion after complexation, indicating stronger interactions between the hydrogens in the water and the CO_2-modified counterions. This also results in a significantly larger number of hydrogen bonds between the CO_2-complexed cy counterion and water. These changes in the water structure around cy are consistent with observations by Wu et al.[16] in which CO_2-complexed ionic liquid tetrabutylphosphonium 2-cyanopyrrolide adsorbs significantly more water than does its uncomplexed counterpart.

Although the position of the first solvation shell of water molecules is unchanged between pro and pro + CO_2, Figure 4 suggests that a larger number of hydrogen atoms occupy this shell around pro + CO_2. This increased occupancy is also manifested as an increase in the number of hydrogen bonds involving pro + CO_2. In this respect, pro-based ionic liquids are expected to behave similarly to glycine-based and alanine-based ionic liquids in interacting more strongly with water in the presence of CO_2.[35]

The hydration environment around the counterions plays a key role in determining their enthalpic and entropic stabilization during solvation. Potential of mean force curves (Figure 5) describe the change in the Gibbs free energy, ΔG, of each counterion as a function of its height, z, above the Gibbs dividing surface at the air/water interface. The lower PMF curve in Figure 5 for the CO_2-complexed tri counterion

Table 1. Physicochemical Parameters of the Surfactants Considered[a]

compound	M_w/(g/mol)	mp/(°C)	cmc/(mM)	β	γ_{2xcmc}/(mN/m)
DTAB	308.34	246	15.1 (14.5[b])	0.72 (0.75[b])	38.3
DTA-tri	296.48	57	11.4	0.77	38.6
DTA-tri CO_2	340.49		8.80	0.26	33.8
DTA-cy	319.53	~49	11.0	0.80	32.5
DTA-cy CO_2	363.54		12.0	0.13	33.7
DTA-pro	342.56	52	8.76	0.26	38.5
DTA-pro CO_2	386.57		10.8	0.07	48.9
C_{12}mim Br	331.35	43	10.3 (11.2[c])	0.65	36.6
C_{12}mim-tri	319.49	35	8.60	0.71	32.1
C_{12}mim-tri CO_2	363.50		8.68	0.10	35.1
DDAB	462.63	158	0.05 (0.07[d])	0.64 (0.53[d])	27.3
DDA-tri	450.79	43	0.04	0.33	25.6
DDA-tri CO_2	494.80				26.0

[a]Values in parentheses are reported in the literature. [b]Data from del Mar Graciani et al.[28] [c]Data from Gu et al.[29] [d]Data from Soltero et al.[30] In the case of DDAB, the cmc actually represents the point at which vesiculation occurs and should be considered a critical vesicle concentration, cvc. Counterion binding should be used as an estimate because demixing can occur above the cmc, affecting the absolute values of β.

DOI: 10.1021/acs.langmuir.7b00679
Langmuir 2017, 33, 7633−7641

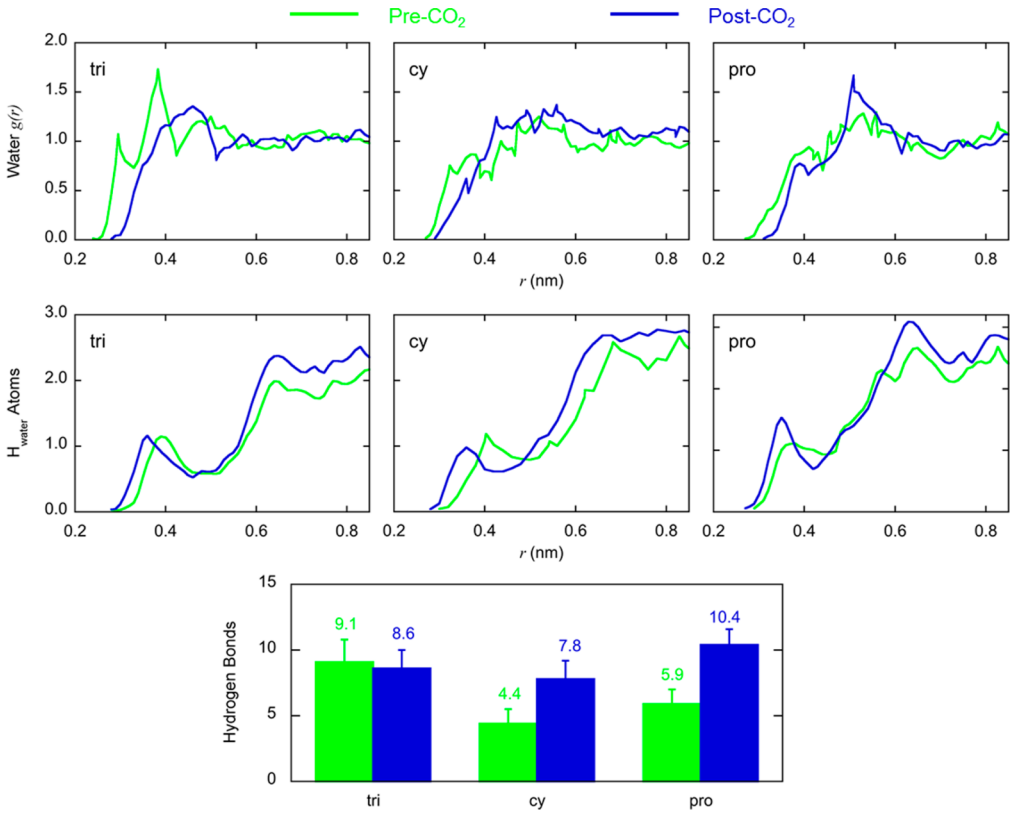

Figure 4. (Top) Structure of water, as quantified by the radial distribution function, around the centers of mass of tri, cy, and pro counterions. (Middle) Number of hydrogen atoms (of water molecules) located at a given distance r from the centers of mass of the counterions. (Bottom) Average numbers of hydrogen bonds between the counterion and the surrounding water molecules before and after complexing with CO_2 (green and blue, respectively).

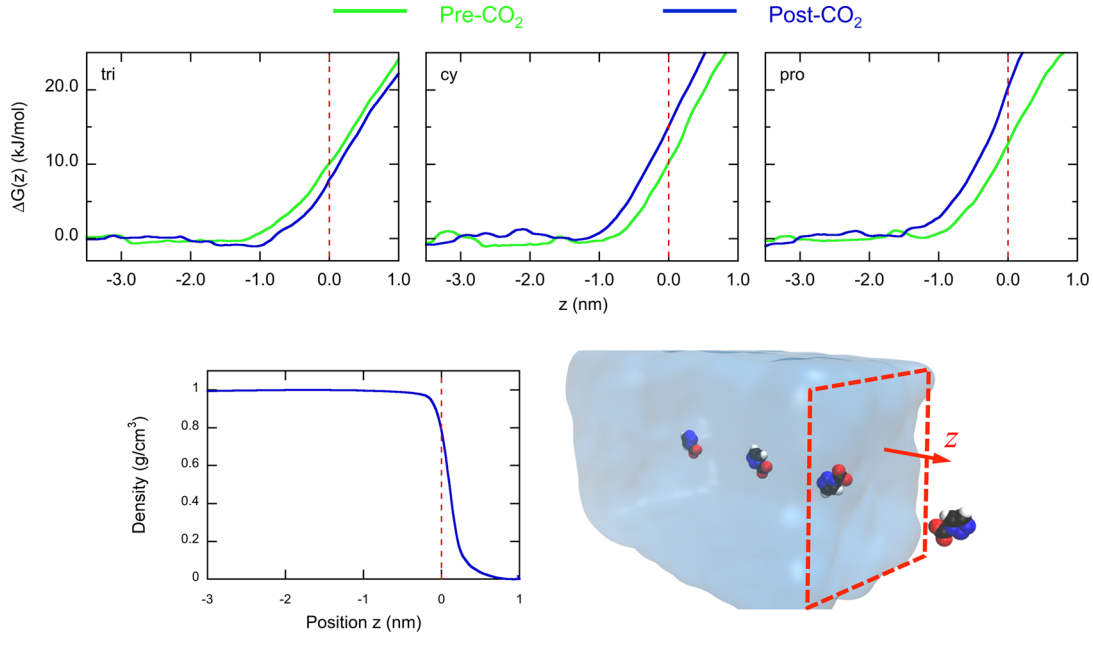

Figure 5. (Top) Free-energy penalties as a function of the height, z, above the Gibbs dividing surface associated with transferring a counterion from a bulk aqueous environment to the air/water interface and beyond (into vacuum) for tri, cy, and pro before and after binding to CO_2 (green and blue, respectively); (bottom left) variation of the density of water as a function of the height above the Gibbs dividing surface (indicated everywhere by the red dashed vertical line); and (bottom right) illustration of the process of transferring a counterion from the bulk aqueous environment to vacuum.

indicates that the free-energy penalty associated with transferring a complexed counterion from a bulk aqueous environment to the air/water interface is lower than the corresponding free-energy penalty for an uncomplexed counterion. In

DOI: 10.1021/acs.langmuir.7b00679
Langmuir 2017, 33, 7633−7641

combination with the stronger attractive interactions between adsorbed counterions and adsorbed surfactants (Figure S3 and Table S3 in the Supporting Information), this increased affinity of tri + CO_2 for the air−water interface suggests that there should be a decrease in the surface tension of tri-based surfactant systems after CO_2 complexation. This result is consistent with our experimental surface tension values at twice the cmc ($\gamma_{2\ cmc}$), where DTA-tri has a surface tension of 38.6 mN m^{-1} and the CO_2-complexed surfactant has a surface tension of 33.8 mN m^{-1} (Table 1). For the cy and pro anions, Figure 5 suggests that complexation with CO_2 leads to reduced affinity of the CO_2-complexed ions for the interface and, consequently, to a greater free-energy penalty accompanying the transfer of the ions from the bulk aqueous solvent to the interface. Combined with the weaker attractive interactions between CO_2-complexed counterions and surfactants adsorbed at the air−water interface (Figure S3 and Table S3 in the Supporting Information), this suggests that CO_2 complexation increases the interfacial tension in these systems. Again, experimentally, we found that $\gamma_{2\ cmc}$ values increase, where in the case of DTA-pro + CO_2 this increase is around 10 mN m^{-1} (~22%). To put this finding in perspective, for straight-chain surfactants, the removal of two methylene groups in the tail increases the surface tension by around 20−30%.[36] *Instead, we can achieve this surface tension increase simply by bubbling CO_2 through the surfactant solution!*

Self-Aggregation—Micelle Structure. We also carried out small-angle neutron scattering (SANS) measurements at different surfactant concentrations to show unambiguously that the surfactants aggregate above the cmc (Figures 6 and S5−S78, Table S4). At 20 times the cmc (used to directly compare all surfactants because DDAB does not show significant scattering intensity below this surfactant concentration), inert parent surfactant DTAB formed ellipsoidal aggregates with a rotational axis of R_a = 16 Å, commensurate with the alkyl chain length (C12), with an aspect ratio of X = 1.5, consistent with literature reports.[37] The size of the ellipsoidal micelle decreased slightly following the exchange of the bromide counterion with triazolide, and the overall micelle charge, ζ, which determines the structure factor (S(Q)) and reflects interparticle interactions, decreased from ~+14 to ~+11. For both counterions, the micelle aggregation number remained approximately constant at around N_{agg} = 50. On sparging of the surfactant solution with CO_2, further reduction in micelle size, with an increase in micelle charge to around +15, was observed. This, in turn, was accompanied by a decrease in the aggregation number of more than 50% to around N_{agg} = 21 (Figures 6). Similar and even more dramatic results were observed for the other surfactants and counterions (Figures S5−S8), with the dichain surfactant exhibiting the clearest change in micelle structure, which morphed from a lamellar-type phase into rods. This is consistent with the reactive counterion causing an increase in the area per headgroup (a_o) of the surfactant and hence a reduction in the value of the packing parameter (N_s) according to $N_s = V/a^*l$, where V is the surfactant tail volume and l is the tail length.[38]

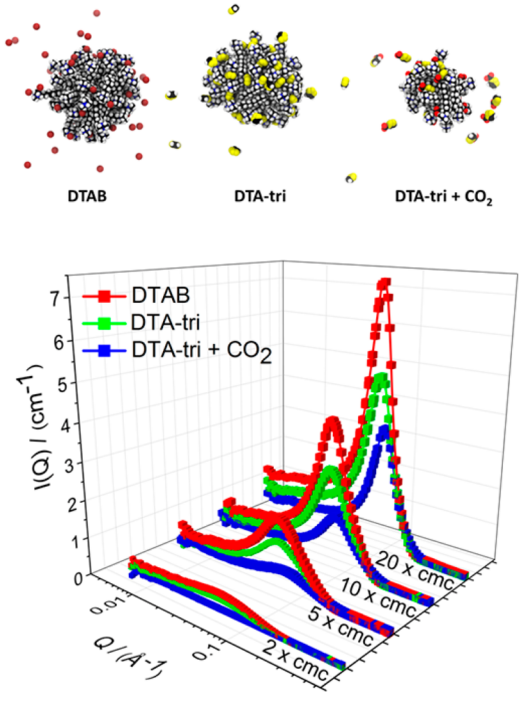

Figure 6. (Top) MD simulation snapshots of DTAB (left), DTA-tri (center), and DTA-tri + CO_2 (right) showing the changes in size and aggregation number, N_{agg}, before and after bubbling with CO_2. The color code used is C (cyan), N (blue), O (red), and H (white). (Bottom) SANS profiles for selected surfactants before and after reaction with CO_2. Lines through the data are fits using the parameters listed in Table S3.

The effects of the anions on the micelle shape, size, and β value are consistent with the Hofmeister series.[39] Although there is still an active debate in the literature about the fundamental physics that controls the position of a given ion in this series, several studies have identified the degree of hydration of an ion as a key contributor.[40] Counterions that are strongly hydrated exhibit a smaller preferential affinity for micelle surfaces and have a smaller degree of counterion binding.[41] As shown in Figure 2, complexation with CO_2 increases the degree of hydration of the counterion, which in turn results in a significantly lower degree of counterion binding, consistent with our measured values for the corresponding micelle (Table 1).

MD simulations of micelles with complexed and uncomplexed counterions also reveal that complexation with CO_2 reduces the interaction energy between the surfactants and the counterions (Table S5), which in turn effectively shifts the distribution of counterions away from the micelle core (Figure S9). The degree of counterion binding, β, in turn, has a pronounced effect on the size of the micelle. An increase in the number of counterions bound to the micelle surface neutralizes more of the micelle surface charge.[42] This reduction in surface charge density enables an increase in micelle size, an effect observed in several other cationic surfactant systems.[41] Therefore, the observed decrease in counterion binding upon CO_2 complexation leads to a decrease in micelle size, which is consistent with our SANS results (Figure 6). These findings allow the control of various colloidal systems such as emulsions stability and microemulsion droplet size (Figures S10 and S11 and Table S6) applicable to a range of colloidal systems.

Reversible DNA Compaction. The most remarkable result obtained in this work, however, involves the reversible compaction of DNA. Initially, cationic surfactants interact with DNA through electrostatic interactions, and it has been postulated that DTAB binds to DNA with one DTAB molecule bound per DNA phosphate group.[40] To induce DNA compaction, a reduction of intramolecular electrostatic forces

DOI: 10.1021/acs.langmuir.7b00679
Langmuir 2017, 33, 7633−7641

by ~90% must occur through charge neutralization.[43] This is followed by hydrophobically driven cooperative binding, which releases both the counterions bound to the DNA and the surfactant molecules into the bulk aqueous environment. The surfactant-induced compaction of DNA leads to a decrease in the complex hydrodynamic radius, with commensurate changes in its translational diffusion coefficient. We determined, using circular dichroism (CD), that our CO_2-reactive surfactant does not disrupt the integral structure of DNA in the stable region of the phase diagram (Figure S12). Circular dichroism shows the characteristic β form,[43] with a negative peak at 248 nm due to the helicity of DNA, a positive peak at 285 nm due to base stacking, and a crossover peak at approximately 260 nm corresponding to the maximum wavelength for normal absorption. The inert DTAB and the CO_2-reactive surfactants DTA-tri (both before and after CO_2 complexation) bind to the DNA duplex with no change in the peak positions, indicating that the β form persisted. The lack of a CD spectrum above 300 nm indicates that no DNA compaction occurred.

Dynamic light scattering (DLS) measurements can probe this change directly and noninvasively, showing coil−globule coexistence in bulk solution. For the relatively small DNA that we studied (2000 bp), it is possible to resolve the fast and slow diffusive modes at a scattering angle of 90°. Therefore, no special analysis was required to extract a hydrodynamic radius from the autocorrelation functions. In particular, DNA extended coils diffuse slowly compared to surfactant-compacted DNA. At a surfactant to DNA base pair ratio (X = [surf]/[PO_4^-]) of 2.48 and relatively low DNA concentration (76 μM, Table S7), DTAB and DTA-tri reduced the hydrodynamic radius of DNA by around 85% (from 196 to ~30 nm). The persistence length of DNA, which is usually 50 nm, with contributions from the intrinsic persistence length (30 nm) and from the charge repulsion of the phosphate groups (20 nm at 0.1 M),[44] is reduced significantly upon binding of the DNA by the surfactant, which alters these charge repulsions. The resulting surfactant−DNA complexes were stable in solution for more than 1 week. This was similar to results reported by Cardenas et al., who showed that CTAB induced a transition of the DNA hydrodynamic radius from about 100 nm to about 50 nm (~50%).[45] In comparison, DTA-tri + CO_2 compacted DNA less efficiently than did inert parent analogue DTAB or DTA-tri, resulting in a 53% reduction in hydrodynamic radius (92 nm) at X = 0.33. Decompaction began at higher surfactant concentrations, and for X > 1.65, full decompaction was observed with the onset of agglomeration. Precipitation, which occurred during the latter stages of compaction, could also be controlled reversibly, an effect that may be exploited in biomolecular extraction and purification operations. It should be noted that the pH of 7.9 of the buffered solution before bubbling with CO_2 decreased to 5.9 after the solution was sparged with CO_2. In this range, DNA is fully charged (pK_A of its phosphate groups is around 1.5). Therefore, it may be assumed that all conformational transformations of the DNA−surfactant conjugates in the system are attributable to CO_2 binding and not to pH changes.[46] As described earlier, the overall compaction process is driven primarily by the large gain in translational entropy associated with the release of the counterions. Consequently, in general, compaction ability is controlled by the position of the counterion in the Hofmeister series, with hydration playing a key role.[47] For the triazolide ion studied here, we can estimate the entropy increase accompanying the release of counterions from the micellar environment by the entropy of solvation calculated in the MD simulations. In particular, our results indicate that the transfer of a tri counterion into a bulk aqueous environment should be accompanied by a significantly greater gain in entropy than that accompanying the transfer of the CO_2-complexed tri + CO_2 counterion. This change in the entropy gain is also consistent with the increased free-energy penalty observed for the transfer of a tri + CO_2 counterion to the air−water interface. This difference in solvation entropy can explain the significant difference in the experimentally observed ability of DTA-tri and DTA-tri + CO_2 to compact DNA.

Fluorescence microscopy was used to detect the compaction of 165.6 kbp T4-DNA molecules directly (Figure 7). The

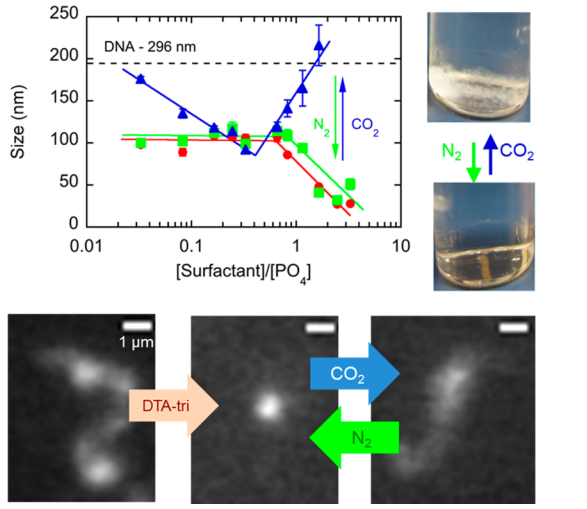

Figure 7. (Top left) DNA compaction by inert DTAB (red circles) and by reactive DTA-tri before (green squares) and after (blue triangles) bubbling with CO_2, as a function of the surfactant to DNA-phosphate molar charge ratio, X, at 25 °C. (Top right) Reversible aggregation of DNA−surfactant conjugates upon bubbling with CO_2 and N_2. (Bottom) Fluorescence images of T4-DNA molecules in (left) the elongated coil form in buffer, (middle) the globular conformation upon addition of DTA-tri, and (right) the re-expansion of DNA after bubbling with CO_2. [T4-DNA] = 0.63 pM.

images clearly show that the extended-coil (wormlike) structures of the native DNA become compacted to form globular objects with no evident coils present after the addition of DTA-tri (X = 26). On the basis of microscopy measurements, it has been reported that large concentrations of CTAB, TTAB, and DTAB, X = 42, 160, and 600, respectively, are necessary to completely condense T4-DNA;[48] therefore, DTA-tri is a more effective compaction agent. Subsequent bubbling of the solutions with CO_2 for 2 min (i.e., an order of magnitude shorter time than in the case of the analogous photoresponsive systems) leads again to the formation of coils (a small fraction of globules coexist).

CONCLUSIONS

We synthesized responsive surfactants with a CO_2-reactive counterion and demonstrated through thermogravimetric analysis CO_2 binding of up to 100 mg CO_2 per g IL, which could be reversed upon changing the gas to N_2. In contrast to previous methodologies,[2−4] in our system the surfactant properties are modulated through counterion manipulation, which allows for a broader selection of responsive surfactants. In particular, by controlling the counterion rather than the head

DOI: 10.1021/acs.langmuir.7b00679
Langmuir 2017, 33, 7633−7641

or tail of the surfactant, reformulation in existing industrial applications (e.g., enhanced oil recovery process) should be more attractive because the synthesis of unusual surfactants will not be required.

The effect of CO_2 binding was twofold. First, it caused charge reorganization, and second, it altered the shape and size of the counterion. Electrical conductivity data showed that these effects caused a reversible shift in the cmc and binding constants, and SANS showed unequivocally that changes in micelle (and vesicle) shape, size, and aggregation number occurred. In particular, for DTA-tri, upon binding to CO_2, intermicellar interactions decreased by more than 20%, and the aggregation number decreased by more than 50% from N_{agg} = 50 to 21. MD simulations corroborated these findings, revealing that complexation with CO_2 reduces the interaction energy between surfactants and counterions, which shifts the distribution of counterions away from the micelle core. In the pursuit of more controlled and sophisticated applications than are possible with other surfactant systems, we also investigated potential applications such as DNA compaction. Here, the new responsive surfactants could compact DNA to below its native persistence length by removing all effective charges. By bubbling with CO_2, this process could be reversed, with the potential to impact research across the biological sciences. For example, polymer analogues with L-proline counterions have already been synthesized as gene vectors.[49] However, the researchers behind these studies did not report any CO_2 responsiveness.

■ ASSOCIATED CONTENT

Supporting Information

The Supporting Information is available free of charge on the ACS Publications website at DOI: 10.1021/acs.langmuir.7b00679.

Analysis of synthesized compounds, electrical conductivity, solvent structure around the counterions, potential of mean force and interfacial tension, surface tensiometry, SANS scattering laws and model fitting, microemulsion formulation, SANS studies of microemulsions, CD studies of DNA−surfactant complexes, DNA stability studies, and DNA compaction studies (PDF)

■ AUTHOR INFORMATION

Corresponding Author

*E-mail: tahatton@mit.edu.

ORCID

Paul Brown: 0000-0002-5660-0377
William T. Heller: 0000-0001-6456-2975
Patrick S. Doyle: 0000-0003-2147-9172
Daniel Blankschtein: 0000-0002-7836-415X
T. Alan Hatton: 0000-0002-4558-245X

Notes

The authors declare no competing financial interest.
#Shared first authorship due to equal contributions.

■ REFERENCES

(1) Ceresana Research. *Market Study on Surfactants*, 2nd ed.; April 2015.
(2) Brown, P.; Butts, C. P.; Eastoe, J. Stimuli-responsive Surfactants. *Soft Matter* **2013**, *9*, 2365−2374.
(3) Liu, Y.; Jessop, P. G.; Cunningham, M.; Eckert, C. A.; Liotta, C. L. Switchable Surfactants. *Science* **2006**, *313*, 958−960.
(4) Lin, S.; Theato, P. CO_2-Responsive Polymers. *Macromol. Rapid Commun.* **2013**, *34*, 1118−1133.
(5) Miguel, M. G.; Pais, A. A. C. C.; Dias, R. S.; Leal, C.; Rosa, M.; Lindman, B. DNA-cationic amphiphile interactions. *Colloids Surf., A* **2003**, *228*, 43−55.
(6) Bilalov, A.; Carlstedt, J.; Krivstova, E.; Lindman, B.; Olsson, U. DNA with amphiphilic counterions: tuning colloidal DNA with cyclodextrin. *Soft Matter* **2012**, *8*, 4988−4994.
(7) Le Ny, A. L.; Lee, T. C. Photoreversible DNA condensation using light-responsive surfactants. *J. Am. Chem. Soc.* **2006**, *128*, 6400−6408.
(8) Zhao, J. K.; Gao, C. Y.; Liu, D. J. The extended Q-range small-angle neutron scattering diffractometer at the SNS. *J. Appl. Crystallogr.* **2010**, *43*, 1068−1077.
(9) Bessis, N.; GarciaCozar, F. J.; Boissier, M. C. Immune responses to gene therapy vectors: influence on vector function and effector mechanisms. *Gene Ther.* **2004**, *11* (Suppl. 1), S10−S17.
(10) Pang, J.; Wang, Y.; Xu, G.; Han, T.; Lv, X.; Zhang, J. Molecular dynamics simulations of SDS, DTAB, and C12E8 monolayers adsorbed at the air/water surface in the presence of DSEP. *J. Phys. Chem. B* **2011**, *115*, 2518−2526.
(11) Darvas, M.; Jorge, M.; Coreiro, M. N. D. S.; Kantorovich, S. S.; Sega, M.; Jedlovsky, P. Calculation of the intrinsic solvation free energy profile of an ionic penetrant across a liquid-liquid interface with computer simulations. *J. Phys. Chem. B* **2013**, *117*, 16148−16156.
(12) Dang, L. X. Computational Study of Ion Binding to the Liquid Interface of Water. *J. Phys. Chem. B* **2002**, *106*, 10388−10394.
(13) Rideg, N. A.; Darvas, M.; Varga, I.; Jedlovszky, P. Lateral dynamics of surfactants at the free water surface: a computer simulation study. *Langmuir* **2012**, *28*, 14944−14953.
(14) Canongia Lopes, J. N.; Deschamps, J.; Padua, A. A. H. Modeling Ionic Liquids Using a Systematic All-Atom Force Field. *J. Phys. Chem. B* **2004**, *108*, 2038−2047.
(15) Yan, F.; Lartey, M.; Damodaran, K.; Albenze, E.; Thompson, R. L.; Kim, J.; Haranczyk, M.; Nulwala, H. B.; Luebke, D. R.; Smit, B. Understanding the effect of side groups in ionic liquids on carbon-capture properties: a combined experimental and theoretical effort. *Phys. Chem. Chem. Phys.* **2013**, *15*, 3264−72.
(16) Wu, H.; Shah, J. K.; Tenney, C. M.; Rosch, T. W.; Maginn, E. J. Structure and Dynamics of Neat and CO2 -Reacted Ionic Liquid Tetrabutylphosphonium 2-Cyanopyrrolide. *Ind. Eng. Chem. Res.* **2011**, *50*, 8983−8993.
(17) Gutowski, K. E.; Maginn, E. J. Amine-functionalized task-specific ionic liquids: a mechanistic explanation for the dramatic increase in viscosity upon complexation with CO_2 from molecular simulation. *J. Am. Chem. Soc.* **2008**, *130*, 14690−704.
(18) Frisch, M. J.; Trucks, G. W.; Schlegel, H. B.; Scuseria, G. E.; Robb, M. A.; Cheeseman, J. R.; Montgomery, Jr., J. A.; Vreven, T.; Kudin, K. N.; Burant, J. C.; Millam, J. M.; Iyengar, S. S.; Tomasi, J.; Barone, V.; Mennucci, B.; Cossi, M.; Scalmani, G.; Rega, N.; Petersson, G. A.; Nakatsuji, H.; Hada, M.; Ehara, M.; Toyota, K.; Fukuda, R.; Hasegawa, J.; Ishida, M.; Nakajima, T.; Honda, Y.; Kitao, O.; Nakai, H.; Klene, M.; Li, X.; Knox, J. E.; Hratchian, H. P.; Cross, J. B.; Bakken, V.; Adamo, C.; Jaramillo, J.; Gomperts, R.; Stratmann, R. E.; Yazyev, O.; Austin, A. J.; Cammi, R.; Pomelli, C.; Ochterski, J. W.; Ayala, P. Y.; Morokuma, K.; Voth, G. A.; Salvador, P.; Dannenberg, J. J.; Zakrzewski, V. G.; Dapprich, S.; Daniels, A. D.; Strain, M. C.; Farkas, O.; Malick, D. K.; Rabuck, A. D.; Raghavachari, K.; Foresman, J. B.; Ortiz, J. V.; Cui, Q.; Baboul, A. G.; Clifford, S.; Cioslowski, J.; Stefanov, B. B.; Liu, G.; Liashenko, A.; Piskorz, P.; Komaromi, I.; Martin, R. L.; Fox, D. J.; Keith, T.; Al-Laham, M. A.; Peng, C. Y.; Nanayakkara, A.; Challacombe, M.; Gill, P. M. W.; Johnson, B.; Chen, W.; Wong, M. W.; Gonzalez, C.; Pople, J. A. *Gaussian 03*, Revision C.02, Gaussian, Inc.: Wallingford. CT, 2004.
(19) Hanwell, M. D.; Curtis, D. E.; Lonie, D. C.; Vandermeersch, T.; Zurek, E.; Hutchison, R. Avogadro: an advanced semantic chemical editor, visualization, and analysis platform. *J. Cheminf.* **2012**, *4*, 17.
(20) Chattoraj, D. K.; Birdi, K. S. *Adsorption and the Gibbs Surface Excess*; Plenum Publishing Company: New York, 1984.

DOI: 10.1021/acs.langmuir.7b00679
Langmuir 2017, 33, 7633−7641

(21) Horinek, D.; Horinek, D.; Herz, A.; Vrbka, L.; Sedlmeier, F.; Mamatkulov, S. I.; Netz, R. R. Specific ion adsorption at the air/water interface: The role of hydrophobic solvation. *Chem. Phys. Lett.* **2009**, *479*, 173−183.
(22) Iyer, J.; Mendenhall, J. D.; Blankschtein, D. Computer simulation-molecular-thermodynamic framework to predict the micellization behavior of mixtures of surfactants: application to binary surfactant mixtures. *J. Phys. Chem. B* **2013**, *117*, 6430−6442.
(23) Abraham, M.; Hess, B.; van der Spoel, D.; Lindahl, E. G. D. *GROMACS 5.0.2 User's Manual*, 2014.
(24) Gurkan, B. E.; Goodrich, B. F.; Minrup, E. M.; Ficke, L. E.; Massel, M.; Seo, S.; Senftle, T. P.; Wu, H.; Glaser, M. F.; Shah, J. K.; Maginn, E. J.; Brennecke, J. F.; Schneider, W. F. J. Molecular design of high capacity, low viscosity, chemically tunable ionic liquids for CO_2 capture. *J. Phys. Chem. Lett.* **2010**, *1*, 3494−3499.
(25) Gurkan, B. E.; de la Fuente, J. C.; Mindrup, E. M.; Ficke, L. E.; Goodrich, B. F.; Price, E. A.; Schneider, W. F.; Brennecke, J. F. Equimolar CO_2 absorption by anion-functionalized ionic liquids. *J. Am. Chem. Soc.* **2010**, *132*, 2116−2117.
(26) Brown, P.; Gurkan, B. E.; Hatton, T. A. Enhanced gravimetric CO_2 capacity and viscosity for ionic liquids with cyanopyrrolide anion. *AIChE J.* **2015**, *61*, 2280−2285.
(27) Chiappe, C.; Pieraccini, D. Ionic liquids: solvent properties and organic reactivity. *J. Phys. Org. Chem.* **2005**, *18*, 275−297.
(28) del Mar Graciani, M.; Muñoz, M.; Rodríguez, A.; Moyá, M. L. Water-N,N-Dimethylformamide Alkyltrimethylammonium Bromide Micellar Solutions: Thermodynamic, Structural, and Kinetic Studies. *Langmuir* **2005**, *21*, 3303−3310.
(29) Gu, Y.; Shi, L.; Cheng, X.; Lu, F.; Zheng, L. Aggregation Behaviour of 1-decyl-3-methylimidazolium Bromide in Aqueous Solution: Effect of Ionic Liquids with Aromatic Anions. *Langmuir* **2013**, *29*, 6213−6220.
(30) Soltero, J. F. A.; Bautista, F.; Pecina, E.; Puig, J. E.; Manero, O.; Proverbio, Z.; Schulz, P. C. Rheological behaviour in the didodecyldimethylammonium bromide/water system. *Colloid Polym. Sci.* **2000**, *278*, 37−47.
(31) Vlachy, N.; Jagoda-Cwiklik, B.; Vácha, R.; Tourad, D.; Jungwirth, P.; Kunz, W. Hofmeister series and specific interactions of charged headgroups with aqueous ions. *Adv. Colloid Interface Sci.* **2009**, *146*, 42−47.
(32) Collins, K. D. Charge density-dependent strength of hydration and biological structure. *Biophys. J.* **1997**, *72*, 65−76.
(33) Ohtaki, H.; Radnai, T. Structure and dynamics of hydrated ions. *Chem. Rev.* **1993**, *93*, 1157−1204.
(34) Thompson, R. L.; Shi, W.; Albenze, E.; Kusuma, V. A.; Hopkinson, D.; Damodara, K.; Lee, A. S.; Kitchin, J. R.; Luebke, D. R.; Nulwala, H. Probing the effect of electron donation on CO_2 absorbing 1,2,3-triazolide ionic liquids. *RSC Adv.* **2014**, *4*, 12748.
(35) Zhang, J.; Zhang, S.; Dong, K.; Zhang, Y.; Shen, Y.; Lv, X. Supported absorption of CO_2 by tetrabutylphosphonium amino acid ionic liquids. *Chem. - Eur. J.* **2006**, *12*, 4021−4026.
(36) Myers, D. *Surfactant Science and Technology*, 3rd ed.; Wiley, 2005.
(37) Bergstrom, M.; Pedersen, J. S. Structure of pure SDS and DTAB micelles in brine determined by small-angle neutron scattering (SANS). *Phys. Chem. Chem. Phys.* **1999**, *1*, 4437−4446.
(38) Israelachvili, J. N.; Mitchell, D. J.; Ninham, B. W. Theory of self-assembly of hydrocarbon amphiphiles into micelles and bilayers. *J. Chem. Soc., Faraday Trans. 2* **1976**, *72*, 1525−1568.
(39) Lo Nostro, P.; Ninham, B. W. Hofmeister Phenomena: An Update on Ion Specificity in Biology. *Chem. Rev.* **2012**, *112*, 2286−2322.
(40) Zavitsas, A. A. Properties of Water Solutions of Electrolytes and Nonelectrolytes. *J. Phys. Chem. B* **2001**, *105*, 7805−7817.
(41) Aswal, V. K.; Goyal, P. S. Role of different counterions and size of micelle in concentration dependence micellar structure of ionic surfactants. *Chem. Phys. Lett.* **2003**, *368*, 59−65.
(42) Srinivasan, V.; Blankschtein, D. Effect of counterion binding on micellar solution behavior: 2. Prediction of micellar solution properties of ionic surfactant-electrolyte systems. *Langmuir* **2003**, *19*, 9946−9961.
(43) Brown, P.; Khan, A. M.; Armstrong, J. P. K.; Perriman, A. W.; Butts, C. P.; Eastoe, J. Magnetizing DNA and Proteins Using Responsive Surfactants. *Adv. Mater.* **2012**, *24*, 6244−6247.
(44) Wasigh, T. A. *The Physics of Living Processes: A Mesoscopic Approach*; Wiley, 2014; p 305.
(45) Cardenas, M.; Schillén, K.; Nylander, T.; Jansson, J.; Lindman, B. DNA Compaction by cationic surfactant in solution and at polystyrene particle solution interfaces: a dynamic light scattering study. *Phys. Chem. Chem. Phys.* **2004**, *6*, 1603−1607.
(46) Mel'nikova, Y. S.; Lindman, B. pH-Controlled DNA Condensation in the Presence of Dodecyldimethylamine Oxide. *Langmuir* **2000**, *16*, 5871−5878.
(47) Dias, R. S.; Pais, A. A. C. C.; Miguel, M. G.; Lindman, B. DNA and surfactants in bulk and at interfaces. *Colloids Surf., A* **2004**, *250*, 115−131.
(48) Jiang, N.; Li, P.; Wang, Y.; Wang, J.; Yan, H.; Thomas, R. K. Micellization of cationic gemini surfactants with various counterions and their interaction with DNA in aqueous solution. *J. Phys. Chem. B* **2004**, *108*, 15385−15391.
(49) Zhang, Y.; Xiang, C.; Lan, J.; You, J.; Chen, L. Synthesis and Biological Applications of Imidazolium-Based Polymerized Ionic iquid as a Gene Delivery Vector. *Chem. Biol. Drug Des.* **2009**, *74*, 282−288.

DOI: 10.1021/acs.langmuir.7b00679
Langmuir 2017, 33, 7633−7641